Comprehensive Characterization of the Double Directional UWB Residential Indoor Channel

Patrice Pajusco, Nadine Malhouroux-Gaffet, Ghaïs El Zein

Comprehensive Characterization of the Double Directional UWB Residential Indoor Channel

P. Pajusco, N. Malhouroux, and G. El Zein

***Abstract*—Recent telecommunication systems exploit the degrees of freedom of the radio propagation channel more and more. Deeper investigations of system performance require realistic channel models. For this purpose, a new MIMO UWB channel sounder is introduced. The novelty is its capacity to estimate simultaneously direction of arrival and departure in 3D, including polarization state information. The second novelty is a new and faster algorithm to estimate the multipath properties of the propagation channel. An extensive measurement campaign is performed in different residential environments and statistical results are provided.**

***Index Terms*—Channel models, direction of arrival estimation, radio propagation, ultra wideband technology.**

I. Introduction

The radio propagation channel has been investigated for many years. Early studies were restricted to statistical path loss models. Rapidly, wideband channel models were required to design digital air interfaces. The simplest one is the tap delay line (TDL) propagation channel model. It was introduced by COST action 207 [1]. The first application was the GSM standard, with a set of channel models using 6 taps: typical urban (TU), bad urban (BU), rural area (RA), etc. TDL propagation models were tuned for most telecommunication systems. The number of taps is proportional to the system bandwidth: 18 for Wi-Fi [2] and up to several hundred for ultra wide band (UWB) systems [3]. To support new multiple input multiple output (MIMO) telecommunication systems, this model was enhanced by including direction of arrival (DOA) and direction of departure (DOD) information on each tap [4].

In the past few years, massive MIMO antenna systems have become a hot topic in wireless research. This concept aims to drastically improve spectral efficiency and reduce transmitted power [5]. Experimental research platforms are already available for realistic investigations [6]. To reduce complexity and improve energy efficiency, spatial modulation could be also another promising candidate for these large array antennas [7]. Whatever the air interface principle, future telecommunication systems will use more and more antennas. Thus, they will be able to exploit simultaneously most of the degrees of freedom of the radio channel. A comprehensive characterization of the radio channel is therefore required to enhance existing propagation channel models. This paper investigates the different dimensions of the static channel simultaneously: complex amplitude, delay, frequency, 3D direction and polarization. In this context, an original UWB-MIMO channel sounder was realized. Its novelty consists in its ability to estimate simultaneously direction of arrival and departure in 3D, including polarization state information. The second novelty is a new and faster algorithm to estimate the multipath properties of the propagation channel. All these results were used experimentally to provide new statistical results of space-time parameters of the propagation channel

The paper is divided as follows. In Section II, a new UWB channel sounder is introduced. Section III proposes a new methodology to extract deterministic and diffuse multipath components. An extensive measurement campaign in three residential environments is detailed in Section IV, in which different examples are provided. The last section is dedicated to the statistical analysis, followed by the conclusion.

II. The UWB Channel Sounder

Experimental investigation of UWB indoor propagation channel requires a channel sounder. An overview of measurement setups is provided in [8] and [9]. In most cases, a vector network analyzer (VNA) is used due to ease of implementation. However, this solution is limited to static configurations. Dynamic channel measurements require dedicated equipment. MIMO measurements are a bit more complex because several links have to be measured at the same time. One solution involves several receivers and orthogonal signals at the transmitter. Switching antennas at the receiver and/or at the transmitter is an alternative to the purely parallel structure. This solution requires a perfect synchronization between the transmitter (TX) and the receiver (RX). However, it also significantly reduces the cost and complexity of the channel sounder and makes it possible to have many antennas. If the overall duration is short enough, the measurements can be considered real-time measurements. Otherwise, the channel environment has to be static. A practical implementation, combining parallel receivers and switching transmitters, is provided in [10].

In this study, the UWB MIMO channel sounder investigates spatial and polarization domains simultaneously.

This paragraph of the first footnote will contain the date on which you submitted your paper for review. This work was supported in part by Orange Labs.

P. Pajusco is with the Microwave Department, Telecom Bretagne Engineering School, Brest, France (e-mail: patrice.pajusco@telecom-bretagne.eu).

N. Malhouroux is with the Orange Labs, Networks and Carriers, Orange Labs, Belfort, France (e-mail: Nadine.malhouroux@orange.com).

G. El Zein is with Institute of Electronics and Telecommunications of Rennes, Rennes, France (e-mail: ghais.el-zein@insa-rennes.fr).

The frequency bandwidth was set between 2.5 and 12.5 GHz. For the sake of clarity, the main features of the equipment, already introduced in [11], are reported here. An overview of the equipment and picture of the system are depicted in Fig. 1 and Fig. 2, respectively. The channel transfer function is estimated using a VNA, which imposes a static environment during measurements. The antennas are identical at the transmitter and the receiver. They combine a virtual circular array and a 5-element array. Such an architecture enables us to electronically beamform in any direction with an arbitrary polarization [12]. All the equipment was piloted by a laptop using Matlab™.

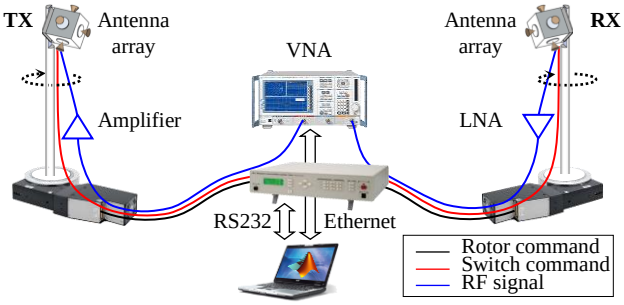

Fig. 1. Overview of the UWB channel sounder

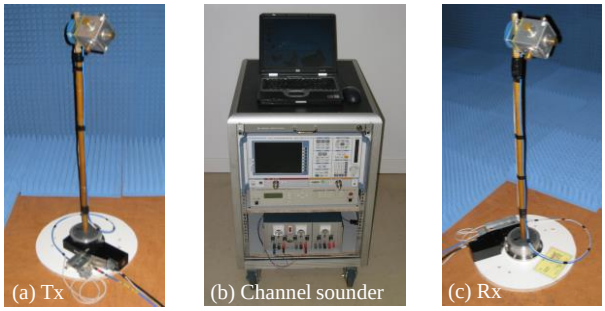

Fig. 2. Picture of the UWB channel sounder

III. Channel Estimation Parameters

A. High-Resolution Algorithm

The simplest way to estimate the multipath radio channel is to use linear methods. For instance, the inverse Fourier transform of the transfer function provides the channel impulse response. Similar transformations are possible to estimate physical paths in the angular domain. These methods are robust whatever the channel, but resolution is limited.

Accuracy can be improved by considering a priori knowledge about the channel. The aim of high-resolution methods is to estimate the parameters of the model accurately. The most common channel model is a set of discrete paths. In practice, the radio channel also includes a diffuse component which can reduce accuracy. In indoor environments, the ratio of the diffuse component ranges from 10 to 30 % in line of sight (LOS) [13, 14] and can reach 90 % in non-line of sight (NLOS) [15]. Even if the accuracy is not as high as expected, high-resolution techniques are often used because the representation of the channel with a limited number of parameters is very convenient for channel modeling.

The MUSIC, ESPRIT, CLEAN and SAGE algorithms are the best-known high-resolution methods. The MUSIC algorithm [16] relies on a subspace decomposition method. Model parameters are obtained by minimizing a numerical function. The resolution is costly in terms of computation and limits the number of problem dimensions to two. When the antenna array has translation invariance, ESPRIT algorithm [17] is very efficient because it provides an analytical solution without requiring any iterative searches. Moreover, the complexity is linear with respect to the number of problem dimensions. However, the set of solutions in each dimension has to be paired, which is not so trivial. The CLEAN method [18], introduced in astronomy, is often used in UWB. With this iterative method, the path parameters of the strongest path are estimated and removed from the original data. The CLEAN method is close to the successive interference cancelation (SIC) method. The last method of this brief overview is the SAGE algorithm [19]. This maximum likelihood method iteratively re-estimates each path parameter, considering the other paths to be perfectly known. The solution is improved after each step. However, this method takes time and requires an initial solution.

B. The CLEAN SVD Algorithm

There is no constraint on the shape of the antenna array when using the CLEAN algorithm. However, above a certain number of dimensions, the algorithm is no longer applicable. A new extension of the CLEAN algorithm is proposed here to deal with the large amount of data provided by this channel sounder. The basic idea is to exploit the strong relationship between the physical properties of paths and the subspace channel radiation pattern introduced in [20]. Actually, there is no one-to-one relationship between a single physical path and a singular value of the MIMO channel matrix. For instance, the radiation pattern of a singular value can beam in different directions corresponding to different paths. However, it always beams approximately in the physical direction of one path. The proposed algorithm is detailed in Fig. 3.

The input data are the MIMO channel impulse responses. The first stage is to find the excess delay of the main path using the power delay profile (PDP). Then, the singular value decomposition (SVD) is applied to the MIMO channel at the delay. It provides the far field associated with the first singular value and enables a rough 3D detection of the direction of departure and arrival of a potential path. Due to the limited beam former resolution, a local optimization is performed to refine the direction estimates. Then, the two arrays are beamed toward these optimal directions to compute the four SISO channels corresponding to each polarization: $h^{VV}, h^{HV}, h^{VH}, h^{HH}$. These four channel impulse responses are interpolated along the delay to get an accurate 2×2 matrix gain of the path. If the amplitude is not high enough, the path is dropped and this excess delay will no longer be scanned. Otherwise, the wideband path contribution is computed and removed from MIMO input data. The procedure is repeated until there is no longer excess delay available.

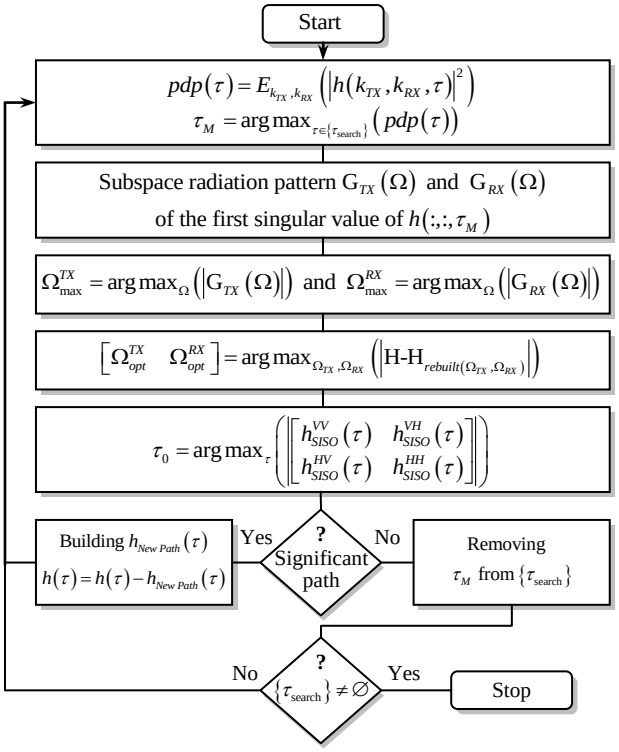

Fig. 3. Principle of the CLEAN-SVD algorithm

C. Diffuse Multipath Component Modeling

The CLEAN-SVD algorithm provides a discrete representation of the radio channel. However, the residual between the measurement and the model is not equal to zero. This error relies on different factors. The most important factor involves the limitations of the propagation model, which is not simply a set of discrete components. However, a part of the residual also comes from the algorithm itself. For instance, the input radiation patterns are not perfectly known. The whole residual, generally called the diffuse multipath component, has to be modeled. Indeed, this component can have a major impact on channel capacity. Reference [21] proposes a global modeling mixing specular components and an omnidirectional diffused component. In [15], authors introduce another model taking into account polarization and different clusters.

The 802.11n MIMO channel model [4] represents the diffuse multipath component by a stochastic process including correlation properties between antenna signals. The principle is briefly recapped here:

$$H = \left(R_{RX}\right)^{1/2} H_{IID}\left(\left(R_{TX}\right)^{1/2}\right)^{T} \quad (1)$$

with

$R_{TX} = \left[\rho_{m,n}^{TX}\right]$ the TX correlation matrix

$R_{RX} = \left[\rho_{m,n}^{RX}\right]$ the RX correlation matrix and

H_{IID} a matrix of independent zero mean, unit variance, complex Gaussian random variables.

The R_{TX} and R_{RX} matrices can be computed directly from MIMO measurements, but the result depends on the antenna array characteristics. It is suitable to derive the correlation coefficients from the power angular spectrum (PAS). Formulas are generally provided in 2D and single polarization [4], but the 3D extension is possible, as follows.

$$\rho_{m,n}^{TX} = \int_{\varphi=0}^{2\pi}\int_{\theta=0}^{\pi}\left(\begin{matrix} G_m^{TX}(\theta,\varphi)\left(G_n^{TX}(\theta,\varphi)\right)^{*} \times \\ G_{PAS}^{TX}(\theta,\varphi)\left(G_{PAS}^{TX}(\theta,\varphi)\right)^{*}\end{matrix}\right)\sin(\theta)\,d\theta\,d\varphi \quad (2)$$

with

$G_{PAS}^{TX}(\theta,\varphi)$ the 3D power angular spectrum at the transmitter

$G_k^{TX}(\theta,\varphi)$ the 3D radiation pattern of the k[th] element.

In this formula, each antenna pattern has the same phase reference location, i.e. the array factor is included in the antenna pattern. This principle simplifies the coefficient computation. The same computation can be performed at the receiver. To compute the experimental value of ρ^{TX} and ρ^{RX} matrices, the power angular spectrum at the TX and RX were estimated using beamforming. An average was performed for all excess delays. As a result, the correlation matrices are supposed the same whatever the excess delay.

D. Model Validation

The two previous sections detailed how to extract the channel parameters of the model, the specular components and the diffuse multipath components. Then, the channel model can be generated by the sum of these two basic propagation channel models. The whole procedure is recapped in Fig. 4.

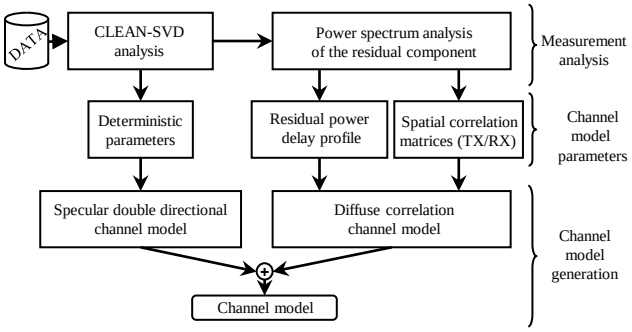

Fig. 4. Procedure to generate the channel model

Different simulations were performed to validate this approach. According to the experimental setup, the MIMO configuration was set to 180×180 with 500 MHz bandwidth.

The first example considered a channel with 20 paths discrete channel model. The path delays were arbitrary distributed within 10 ns delay. The direction of departure, the direction of arrival and the polarization of each ray were chosen arbitrary. Noise was applied to reach a 20 dB signal to noise ratio. The CLEAN-SVD algorithm was applied. Contrary to SAGE algorithm, the CLEAN-SVD does not require any iteration process. The results are provided in Table I. In this simple multipath configuration, a good agreement between model (in black) and estimate (in red) is found. Direction of arrival and departure resolution is better than a degree and amplitude accuracy is better than 0.5 dB. The channel capacity was computed and the result is the same with the channel model and its estimate with CLEAN-SVD.

TABLE I
RESULTS OF CLEAN-SVD WITH NOISY DISCRETE CHANNEL MODEL

Delay	DOA		DOD		g_{VV}	g_{VH}	g_{HV}	g_{HH}
ns	θ	φ	θ	φ	dB	dB	dB	dB
10.57	76.1°	-63.5°	138.0°	-134.2°	-6.5	-4.3	-1.1	-6.3
10.58	76.0°	-63.0°	138.0°	-135.0°	-6.4	-4.3	-1.1	-6.3
10.58	86.4°	76.2°	110.1°	-134.7°	0.0	-2.6	-1.3	-7.9
10.58	86.0°	75.0°	110.0°	-135.0°	-0.1	-2.6	-1.1	-7.6
11.20	133.9°	-176.0°	88.1°	-168.5°	-0.7	1.3	-2.1	0.4
11.18	134.0°	-177.0°	88.0°	-168.0°	-0.4	1.2	-2.6	0.3
11.26	50.4°	-26.3°	111.4°	-69.2°	-6.3	-8.8	-4.5	-6.3
11,26	50.0°	-27.0°	111.0°	-69.0°	-6.3	-8.9	-4.5	-6.3
⋮	⋮	⋮	⋮	⋮	⋮	⋮	⋮	⋮
16.01	88.6°	-43.8°	169.6°	77.0°	1.7	-10.8	-0.2	-5.0
16.03	89.0°	-45.0°	170.0°	78.0°	1.3	-10.6	-0.1	-5.0
⋮	⋮	⋮	⋮	⋮	⋮	⋮	⋮	⋮

The second example is more realistic. Two components with identical power level are mixed: a discrete part and a diffuse multipath component. The discrete path is composed of 3 paths. Two of them are located at the same delay. The diffuse part is spread in delay and in angular domain. According to experimental results [21], an exponential and a von Mises-Fisher distribution were used in delay and angular domain respectively. This DOA-DOD configuration is recapped in Fig. 5. The three crosses represent the locations of the deterministic paths. The color enables pairing between transmitter and receiver.

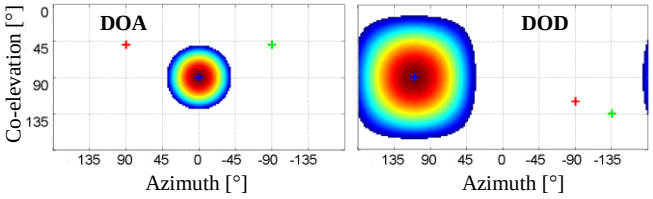

Fig. 5. Configuration of the model

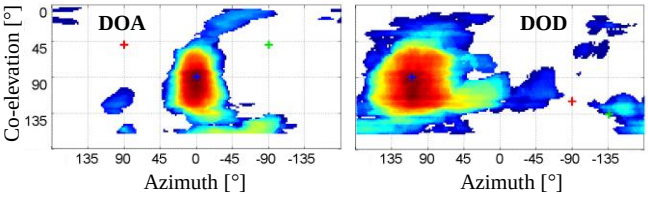

Fig. 6. Estimate of the discrete and diffuse component

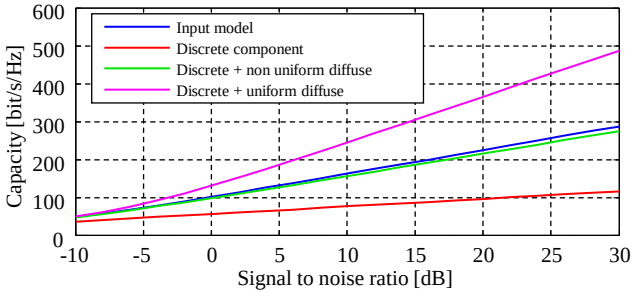

Fig. 7. Water filling channel capacity: Model and its estimate

The estimate of the discrete paths (CLEAN-SVD) and diffuse multipath components is depicted in Fig. 6. The deterministic part is estimated with the same accuracy as the previous example. The two diffuse components are found at the right place. The spread are similar but the shape is not exactly the same as the model. Due to the random process, each simulation leads to a different results but the general shape is the same.

To quantify the accuracy of this model, the channel capacity was computed. The water filling capacity was performed considering the whole 180×180 antenna array. The result is depicted in Fig. 7. It shows that the lack of diffuse multipath component leads to underestimate the channel capacity. Contrariwise, simple uniform distribution channel model overestimates the channel capacity. Taking into account a non-uniform diffuse multipath component provides approximately the same capacity. This channel decomposition will be used in next section to analyze MIMO channel measurements.

IV. PROPAGATION MEASUREMENTS

A. Measurement Setup

Propagation measurements were carried out with the channel sounder presented in Section II. Thus, the obtained data aim to provide new statistical results to improve existing channel models. Due to the massive deployment of personal telecommunication systems, we focused on residential environments. The frequency bandwidth was set between 2.5 and 12.5 GHz. This includes the whole allocated bandwidth of UWB systems. The TX and RX antenna system of the virtual array was placed in 60 locations along a circle. Only three of the five antennas were used to reduce the measurement duration. This configuration is equivalent to a 180×180 MIMO transmission and required about 4 hours to be captured. To avoid variability, measurements were performed without people in the buildings, i.e. during the night or the weekend.

B. Measurement Description

For the current study, 32 measurement locations were investigated, representing more than 1 million channel impulse responses, 30 GB of raw data and 130 hours of actual measurements. To facilitate the reuse of such data, each environment was modeled in 3D. A panoramic picture was shot at each measurement location, which provides an accurate view of the environment during measurement. This makes it possible to superimpose the direction of the arrival/departure results on the panoramic pictures, which is very convenient in analyzing spatial spreading as explained in [22]. Such an approach was first used in [23] to analyze double directional outdoor measurements. The following sections detail the three different environments.

1) Meeting room

Because of its simplicity, the meeting room environment was used to validate the channel sounder. This room (10.6 m × 6.8 m) is furnished mainly with a long table surrounded by chairs. The TX and RX face each other, with one at each end of the table.

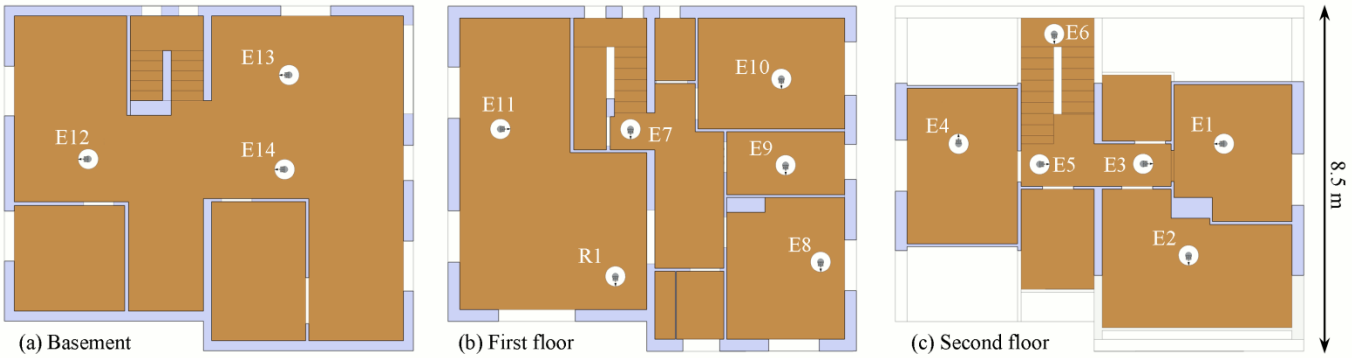

Fig. 8. Measurement location in residential house environment

2) Apartment

This residential apartment is located inside the Orange Labs premises. It represents a typical French apartment and was designed according to the results of an extensive statistical study. This furnished apartment consists of two bedrooms, a kitchen, an office and a large living room. Thirteen different transmitter locations were investigated. The whole setup is depicted in Fig. 9.

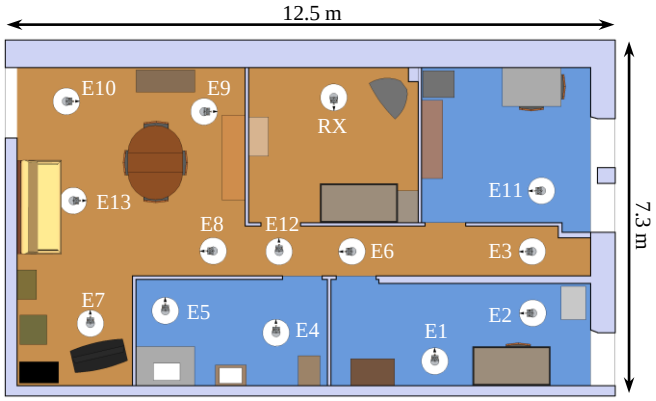

Fig. 9. Measurement location in residential apartment environment

3) Residential House

It is also important to characterize the residential house environment. Moreover, statistical data collected in this type of configuration are not often reported in the literature. Measurements were performed in a house built in the 1970s. The inner walls are made of brick and weight-bearing walls are made of concrete. The receiver was set on the first floor and the transmitter was placed in various locations on each floor. This made it possible to investigate radio links between floors, which is not so frequent in the literature. The description of the environment and the 14 measurement locations are reported in Fig. 8. The E1 location was measured twice to check the consistency of the measuring equipment.

C. Measurement Examples

Such measurements contain a large amount of information. To present some examples, the most important parameters were gathered on a single page. Some explanations are useful to benefit of the full information. The configuration of the measurement is given on in the top right of the figure. Significant parameters are provided such as TX-RX distance, link condition, excess delay spread and angular spread at TX and RX. These angular spread parameters are computed in 3D according to [24]. This explains that these parameters have no unit.

The figure a) represents the power delay profile, which is computed by averaging the 180×180 instantaneous channel impulse responses. The vertical red line indicates the specific excess delay values used to analyze the direction of departure and arrival. The figure b) represents four examples of spatial distribution of power at the transmitter and the receiver. The results are superimposed on the panoramic picture at the transmitter and receiver. The geometrical direction of the transmitter/receiver is also indicated, which is very convenient in NLOS situation. The figure c) presents the average over all the excess delay values. At last, the figure d) shows the main discrete components obtained from the CLEAN SVD algorithm. The color circle enables pairing TX and RX paths.

1) LOS scenario

This measurement was performed in LOS situation in the meeting room. The whole results are provided in Fig. 10. As expected, the LOS path is the strongest one and comes from the opposite antenna. Several reflections are visible especially one from a metallic whiteboard (the other coming from walls). Even in LOS situation, the average power spatial distribution highlights diffuse phenomena around main paths.

2) NLOS scenario with TX and RX on the same floor

This second example was performed in NLOS situation in house environment. The whole results are provided in Fig. 11. The LOS path does not appear on the power delay profile. The strongest path comes from diffraction on the metallic door frame. In fact, most of paths come from frame of the opened door. This clearly appears on the average power spatial distribution where the shape of the power is similar with the shape of the door. The second contribution comes from wall reflection.

3) NLOS scenario with TX and RX on different floor

This last example was performed between floors. The whole results are provided in Fig. 12. The analysis at the first delay confirms that this path corresponds to the direct path.

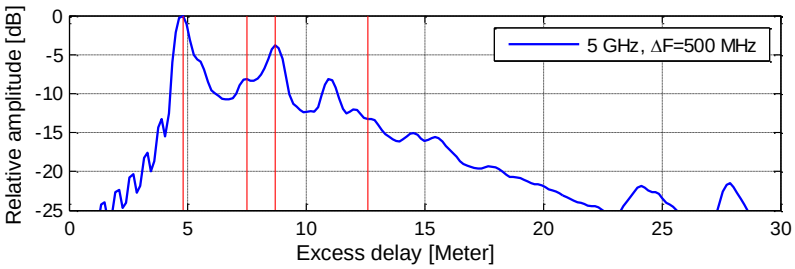

Measurement location	: LouisNeel
Environment	: Meeting room
Link condition	: LOS
TX-RX distance	: 4.8 m
Delay spread	: 13.62 ns
3D angular spread at TX	: 0.76
3D angular spread at RX	: 0.90

(a) Power delay profile at the measurement location

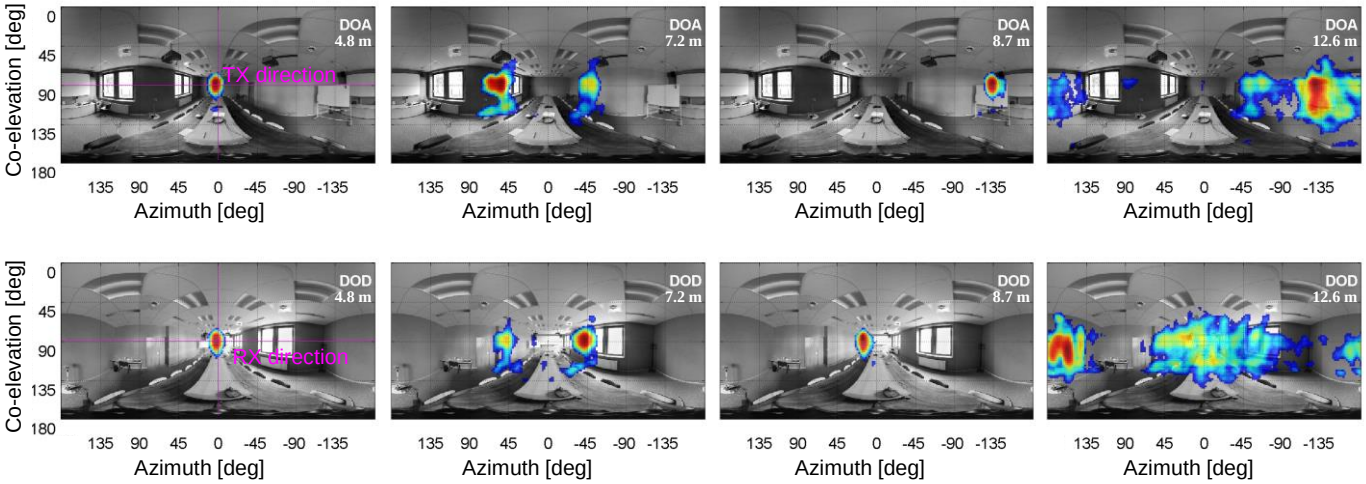

(b) Power spatial distribution for different excess delays : 4.8 m / 7.2 m / 8.7 m / 12.6 m

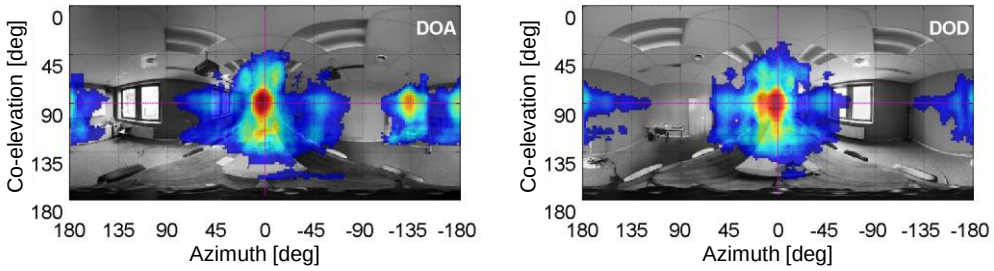

(c) Average power spatial distribution

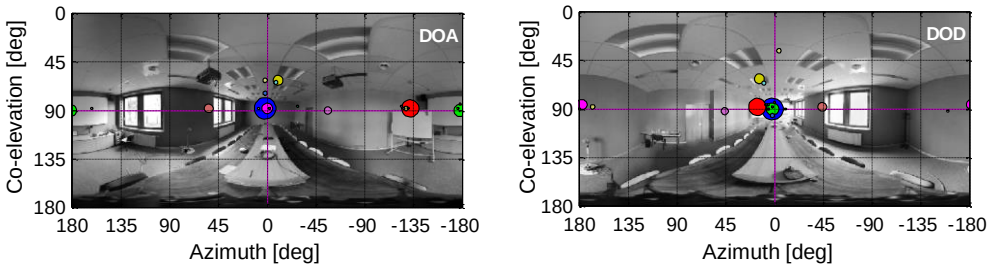

(d) Spatial distribution of deterministic paths

Fig. 10. Measurement example in meeting room environment

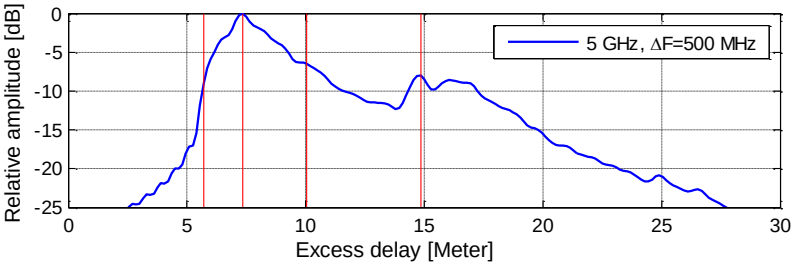

Measurement location	: E8R1
Environment	: House
Link condition	: NLOS
TX-RX distance	: 5.6 m
Delay spread	: 13.39 ns
3D angular spread at TX	: 0.94
3D angular spread at RX	: 0.79

(a) Power delay profile at the measurement location

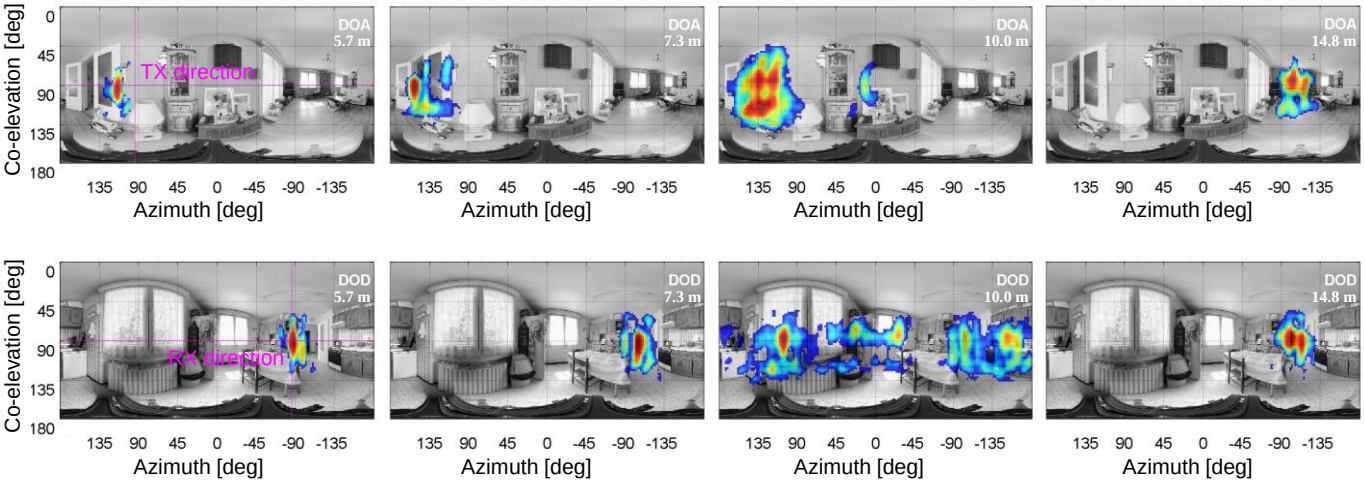

(b) Power spatial distribution for different excess delays : 5.7 m / 7.3 m / 10.0 m / 14.8 m

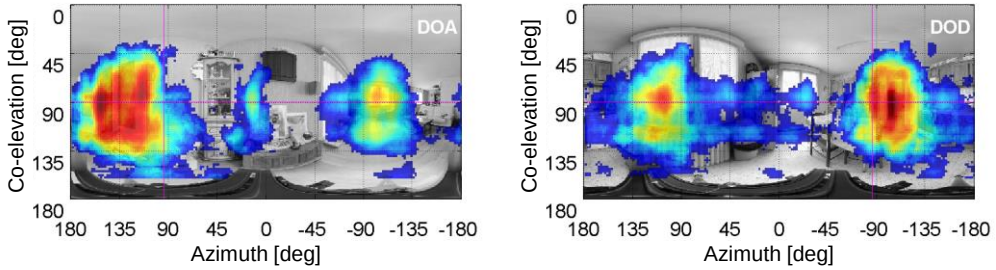

(c) Average power spatial distribution

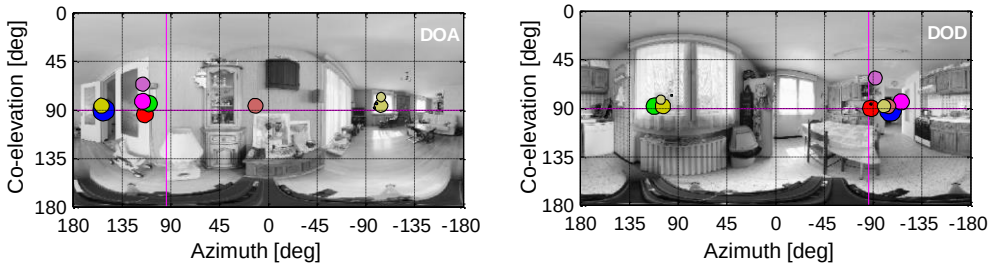

(d) Spatial distribution of deterministic paths

Fig. 11. Measurement example in residential environment (TX and RX on the same floor)

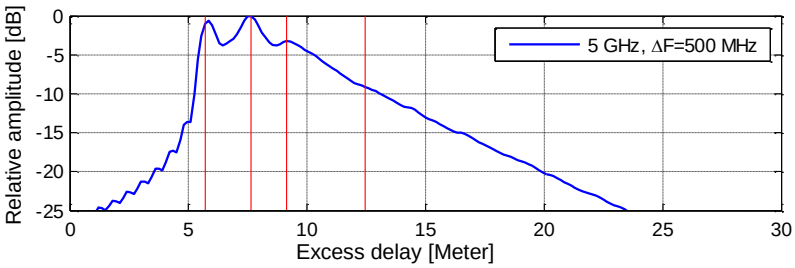

Measurement location	: E4R1
Environment	: House
Link condition	: NLOS
TX-RX distance	: 5.3 m
Delay spread	: 9.28 ns
3D angular spread at TX	: 0.81
3D angular spread at RX	: 0.86

(a) Power delay profile at the measurement location

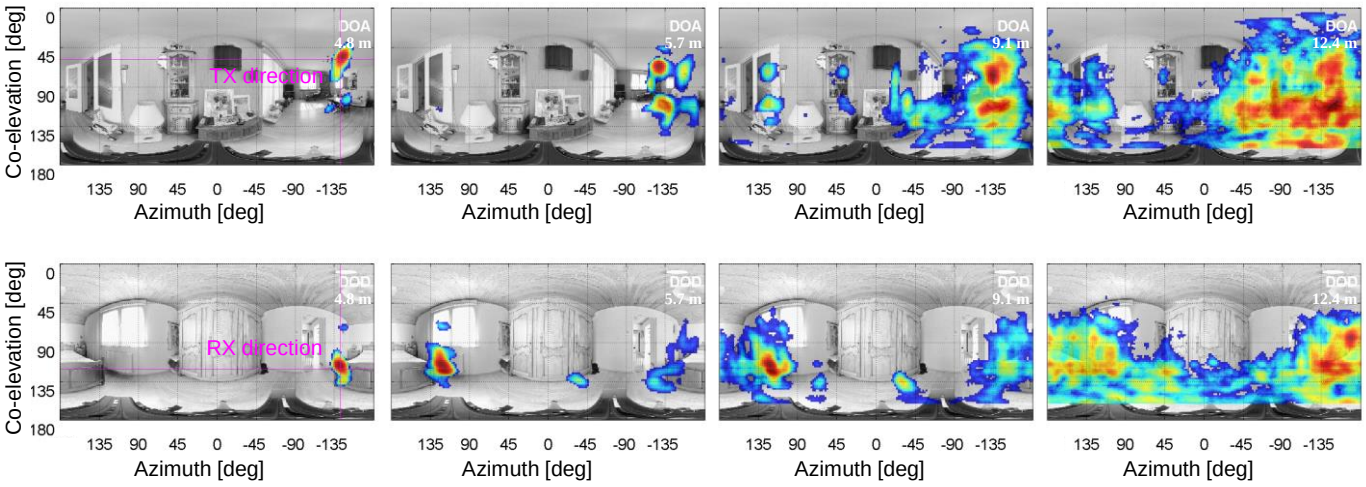

(b) Power spatial distribution for different excess delays : 5.7 m / 7.6 m / 9.1 m / 12.4 m

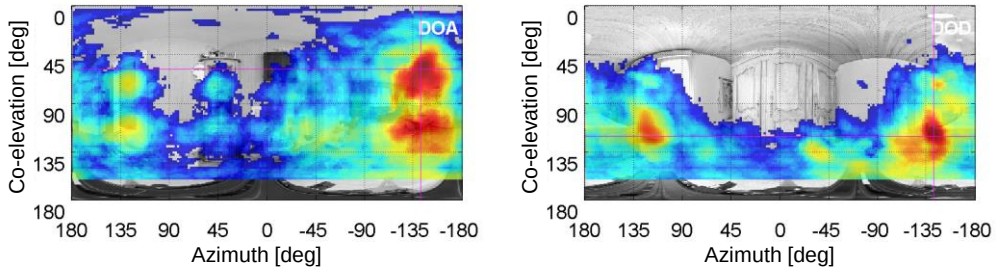

(c) Average power spatial distribution

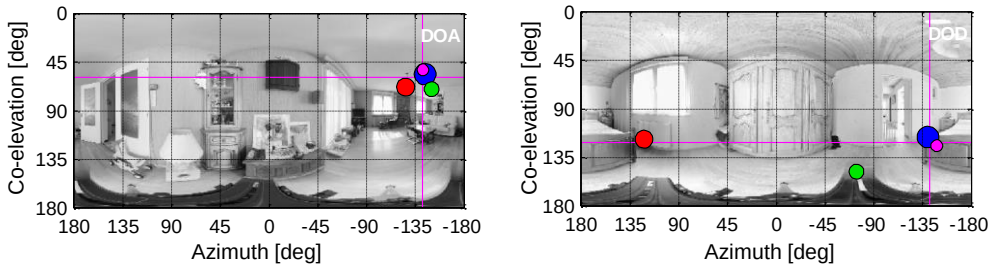

(d) Spatial distribution of deterministic paths

Fig. 12. Measurement example in residential environment (TX and RX on two different floors)

Indeed, the LOS direction fit to the TX-RX direction. The other delay examples present more paths and spatial spreading, even if they are at a local maximum of the power delay profile. In fact, electromagnetic waves experience much more complex mechanism which explains the increase of the scattering component. Nevertheless, main power comes approximately from the LOS direction.

V. Statistical Results

A. Path Loss

Statistical path loss channel models are very convenient to evaluate the system link budget without any geographical data base. A wide set of models are available in the literature. Most of them are dedicated to the single frequency band. This study focuses on frequency dependence, especially when the transmission link involves several floors.

The path loss can be modeled statistically by (3). The distance and frequency are each taken into account with a power exponent parameter.

$$L(f,d) = L_o(f_0,d_0).\left(\frac{d}{d_0}\right)^n \left(\frac{f}{f_o}\right)^{2\kappa+2} \quad (3)$$

with

n the distance dependence coefficient

d_0 the reference distance

κ the frequency dependence coefficient

f_0 the center frequency

The frequency dependence of the path loss depends on the physical properties of the environment. It also depends on the type of interaction. For instance, the analytical expression of the diffraction attenuation involves the frequency parameter [25]. The antenna pattern can also modify the path loss when the frequency changes [26].

To estimate the κ parameter in the different indoor environments, the path loss was estimated for each frequency by averaging over the different MIMO links. The antenna effects were minimized by removing the antenna gain of the LOS at each frequency.

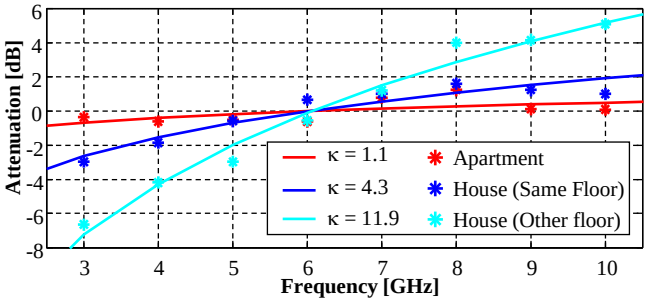

Fig. 13. Path loss versus frequency

The basic frequency dependence $20\log_{10}(f)$ was also removed from the measurements. It should be noted that the κ value represented approximately the variation in dB between 3 and 10 GHz of the remaining attenuation. The κ values in the house and apartment environments are depicted in Fig. 13. The meeting room configuration, which is not reported, is similar to the apartment configuration.

In the apartment environment, the κ parameter value is 1.1, which is consistent with the IEEE 802.15.4a channel model [3]. In the house environment, the value is higher. It increases from 4.3 when the TX and RX are on the same floor, to 11.9 when they are on different floors. This increase relies on the properties of the building materials, whose losses increase with frequency, especially the concrete slabs [27].

B. Delay Spreading

Delay dispersion is important for wideband channel models. The median delay spread was computed in the different environments at different frequencies. Measurement results in an anechoic chamber were also performed to get reference values. In the house environment, a single curve is reported, because results are similar on the different floors. The results are depicted in Fig. 14. A linear decrease of the delay spread can be observed. The same trend with frequency bands was reported in [28, 29]. In our experiment, the slope of the delay spread parameter was estimated at -2% per GHz. For a single location, the frequency correlation is very high. In the apartment and house environments, with 4 GHz spacing, the values are 93% and 87%, respectively. Other values of frequency spacing are available in Table II.

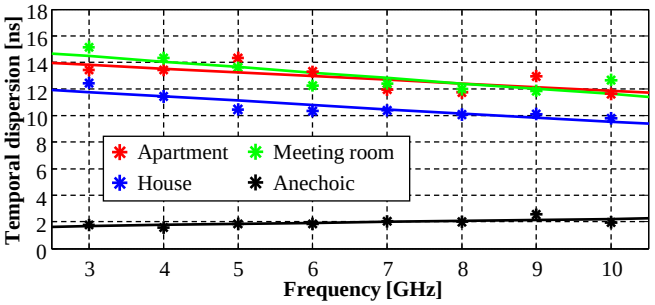

Fig. 14. Delay spread parameter versus frequency

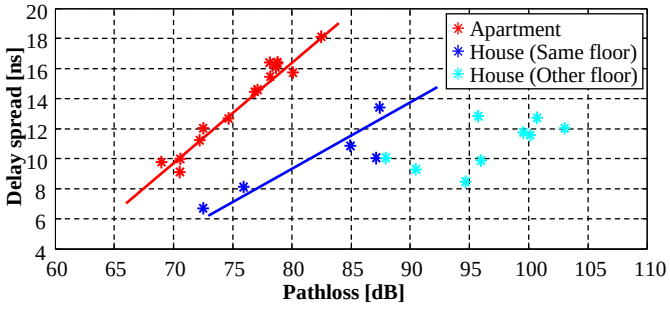

Fig. 15. Delay spread parameter versus path loss parameter

From one location to another, the delay spread can change a great deal. Its value depends on the amplitude of the direct path versus the power of the multipath components. The path loss of the direct path is mainly due to transmission through walls and concrete slabs. If the multipath component is assumed constant whatever the location, the delay spread should be correlated with the path loss. The behavior is confirmed in Fig. 15, especially in the apartment environment. On the same floor in the house environment, the trend seems to be the same, but there are not enough measurements to

conclude. In the case of measurement on different floors, the direct path is highly attenuated by concrete slab transmission. Thus, just the multipath component remains and the correlation no longer exists.

C. Spatial Spreading

Spatial spreading is the key parameter in the double-directional channel model. Many statistical results are available in 2D in the azimuth plane [30]. However, results in the elevation plane or at different frequencies are rare. This experiment makes it possible to provide such information. Due to the symmetry of our configuration and the small number of measurement points, results at RX and TX are mixed. Azimuth and elevation spread are depicted in Fig. 16 and Fig. 17, respectively. The higher the frequency, the lower the azimuth spread and elevation spread.

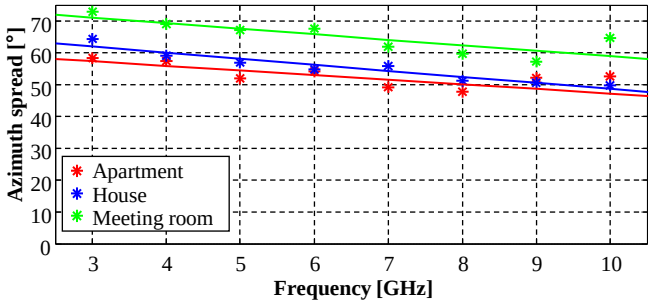

Fig. 16. Azimuth spread parameter versus frequency

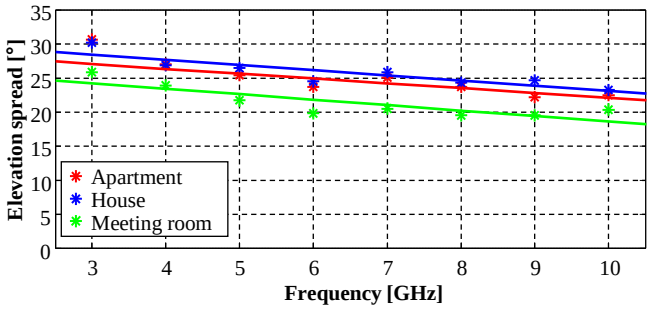

Fig. 17. Elevation spread parameter versus frequency

TABLE II
FREQUENCY CORRELATION OF DISPERSION PARAMETERS

Dispersion Domain	Environment	Frequency correlation $\Delta f = 1$ GH:	$\Delta f = 2$ GHz	$\Delta f = 4$ GHz	$\Delta f = 6$ GHz
Delay	House	95.7 %	93.3 %	88.8 %	87.0 %
Delay	Apartment	97.3 %	96.5 %	95.6 %	93.0 %
Azimuth	House	96.4 %	94.2 %	91.6 %	90.3 %
Azimuth	Apartment	89.3 %	85.2 %	77.2 %	66.8 %
Elevation	House	98.3 %	96.9 %	95.9 %	94.8 %
Elevation	Apartment	88.6 %	85.7 %	83.9 %	74.8 %

If a linear relation is considered, the slope is -0.76° per GHz and -1.76° per GHz for the elevation and azimuth spread, respectively. Due to these low values, it is possible to express the decrease in terms of percentage. In this case, the slope is about -3%/GHz for both parameters.

The frequency correlation parameter is very high especially in the house environment. Values for different frequency spacing are presented in Table II.

VI. CONCLUSION

A UWB MIMO channel sounder and the CLEAN-SVD algorithm were introduced. They make it possible to extract all the characteristics of the UWB static channel: path gain (including polarization state information), path excess delay, and 3D path directions at both the transmitter and the receiver. Measurement campaigns were performed in different residential areas. Examples were detailed to highlight propagation mechanisms. This statistical analysis in residential configuration provided new results. The higher the frequency, the lower the channel spreading parameter values: -2% per GHz for delay spread and -3% for azimuth and elevation spread. A significant correlation between path loss and delay spread was highlighted when transmitter and receiver are located on the same floor. A path loss model, including frequency dependence, was also proposed. These results will help to refine existing UWB MIMO channel models in residential environments. Future work will focus on outdoor–to-indoor link configurations.

ACKNOWLEDGMENT

The authors wish to thank Y. Chartois and A. Bazi for their support in implementing part of the acquisition and post processing software respectively, C. Sabatier for designing the UWB monopole antenna and A. Johansen for her English review.

REFERENCES

[1] COST207, Ed., *Digital Land Mobile Radio Communications, Final report*. Luxembourg, 1989, p.^pp. Pages.

[2] J. Medbo and P. Schramm, "Channel Models for HIPERLAN/2 in different Indoor Scenarios," *ETSI BRAN 3ERI085B*, 1998.

[3] A. F. Molisch, K. Balakrishnan, C. Chong, S. Emami, A. Fort, J. Keredal, *et al.*, "IEEE 802.15.4a channel model - final report," in *IEEE P802.15 Working Group for WPANs, Technical Report IEEE P802.15-04/0662r1-SG4a*, 2004.

[4] V. Erceg, L. Schumacher, P. Kyritsi, A. Molish, D. S. Baum, and al., "TGn channel models," *IEEE 802.11-03/940r9*, may 2004 2004.

[5] F. Rusek, D. Persson, L. Buon Kiong, E. G. Larsson, T. L. Marzetta, O. Edfors, *et al.*, "Scaling Up MIMO: Opportunities and Challenges with Very Large Arrays," *Signal Processing Magazine, IEEE*, vol. 30, pp. 40-60, 2013.

[6] C. Shepard, H. Yu, and L. Zhong, "ArgosV2: A Flexible Many-Antenna Research Platform," presented at the Conf. Mobile Computing and Networking (MobiCom), Miami, Florida, 2013.

[7] M. Di Renzo, H. Hass, and A. Ghrayeb, "Spatial Modulation for MIMO Wireless Systems," presented at the IEEE Wireless Communications and Networking Conference, Shanghai, China,, 2013.

[8] P. Pagani, F. Tchoffo Talom, P. Pajusco, and B. Uguen, *Ultra-Wideband Radio Propagation Channels*: Willey, 2008.

[9] J. Ahmadi-Shokouh and R. C. Qiu, "Ultra-wideband (UWB) communications channel measurements – a tutorial review," *Int. J. of Ultra Wideband Communications and Systems*, vol. Vol.1, pp. 11 - 31, 2009.

[10] M. Kmec, J. Sachs, P. Peyerl, P. Rauschenbach, R. Thomä, and R. Zetik, "A novel Ultra-Wideband Real-Time MIMO Channel

Sounder Architecture," presented at the General Assembly Int. Union of Radio Science (URSI), New Delhi, India, 2005.

[11] N. Malhouroux, E. Haddad, L. Ndiaye, and P. Pajusco, "Capacity of UWB propagation channel in outdoor to indoor configuration," in *European Conference on Antennas and Propagation (EuCAP)*, Rome, 2011.

[12] P. Pajusco, C. Sabatier, G. Tesserault, and N. Malhouroux, "Novel Array Structure for Space-Time Characterization of the UWB Channel," in *PIMRC*, Cannes, 2008.

[13] K. Haneda, J. Takada, and T. Kobayashi, "Double Directional UltraWideband Channel Characterization in a Line-of-Sight Home Environment," *IEICE Trans. Fundamentals*, pp. 2264-2271, September 2005 2005.

[14] H. Tsuchiya, K. Haneda, and J. Takada, "UWB Indoor Double-Directional Channel Sounding for Understanding the Microscopic Propagation Mechanisms," in *WPMC*, Italy, 2004, pp. 95-99.

[15] J. Salmi, J. Poutanen, K. Haneda, A. Richter, V. M. Kolmonen, P. Vainikainen, *et al.*, "Incorporating diffuse scattering in geometry-based stochastic MIMO channel models," in *European Conference on Antennas and Propagation (EuCAP)*, Barcelona, 2010.

[16] R. Schmidt, "Multiple emitter location and signal parameter estimation," *Antennas and Propagation, IEEE Transactions on*, vol. 34, p. 276, 1986.

[17] R. Roy and T. Kailath, "ESPRIT-estimation of signal parameters via rotational invariance techniques," *Acoustics, Speech and Signal Processing, IEEE Transactions on*, vol. 37, p. 984, 1989.

[18] J. M. Cramer, R. A. Scholtz, and M. Z. Win, "On the analysis of UWB communication channels," in *Military Communications Conference Proceedings, 1999. MILCOM 1999. IEEE*, 1999, p. 1191.

[19] B. H. Fleury, M. Tschudin, R. Heddergott, D. Dahlhaus, and K. Ingeman Pedersen, "Channel parameter estimation in mobile radio environments using the SAGE algorithm," *Selected Areas in Communications, IEEE Journal on*, vol. 17, p. 434, 1999.

[20] P. Pajusco and N. Malhouroux, "Relationship between physical and subspace propagation channels, Simulation and experimental study," in *Personal, Indoor and Mobile Radio Communications*, Istanbul, Turkey, 2010.

[21] N. Czink, A. Richter, E. Bonek, J.-P. A. N. J.-P. Nuutinen, and J. A. Y. J. Ylitalo, "Including Diffuse Multipath Parameters in MIMO Channel Models," in *Vehicular Technology Conference, 2007. VTC-2007 Fall. 2007 IEEE 66th*, 2007, p. 874.

[22] J. M. Conrat and P. Pajusco, "A versatile propagation channel simulator for MIMO link level simulation," in *COST 273*, Paris, 2003.

[23] B. H. Fleury, P. Jourdan, and A. Stucki, "High-resolution channel parameter estimation for MIMO applications using the SAGE algorithm," in *Broadband Communications, 2002. Access, Transmission, Networking. 2002 International Zurich Seminar on*, 2002, pp. 30-1.

[24] B. H. Fleury, "First- and second-order characterization of direction dispersion and space selectivity in the radio channel," *Information Theory, IEEE Transactions on*, vol. 46, p. 2027, 2000.

[25] R. C. Qiu and I. T. Lu, "Wideband wireless multipath channel modeling with path frequency dependence," in *Communications, 1996. ICC 96, Conference Record, Converging Technologies for Tomorrow's Applications. 1996 IEEE International Conference on*, 1996, p. 277.

[26] P. Pajusco and P. Pagani, "Frequency Dependence of The UWB Indoor Propagation Channel," in *European Conference on Antennas and Propagation (EuCAP)*, Edinbourg, 2007.

[27] G. Tesserault, N. Malhouroux, and P. Pajusco, "Determination of Material Characteristics for Optimizing WLAN Radio," in *ECWT* Munich 2007

[28] P. Nobles and F. Halsall, "Delay spread and received power measurements within a building at 2GHz, 5 GHz and 17 GHz," in *International Conference on Antennas and Propagation*, Edinburgh, 1997.

[29] G. J. M. Janssen and R. Prasad, "Propagation measurements in an indoor radio environment at 2.4 GHz, 4.75 GHz and 11.5 GHz," in *Vehicular Technology Conference, 1992, IEEE 42nd*, 1992, p. 617.

[30] COST2100, "European Co-operation in Pervasive Mobile & Ambient Wireless Communications," 2010.